

submitted to *The Astrophysical Journal* (2016 May 20)

# Quantum Suppression of Alignment in Ultrasmall Grains: Microwave Emission from Spinning Dust will be Negligibly Polarized

B. T. Draine

Princeton University Observatory, Peyton Hall, Princeton, NJ 08544-1001, USA;  
draine@astro.princeton.edu

Brandon S. Hensley

Jet Propulsion Laboratory, California Institute of Technology, 4800 Oak Grove Drive, Pasadena  
CA 91109, USA

## ABSTRACT

The quantization of energy levels in very nanoparticles suppresses dissipative processes that convert grain rotational kinetic energy into heat. For grains small enough to have  $\sim$ GHz rotation rates, the suppression of dissipation can be extreme. As a result, alignment of such grains is suppressed. This applies both to alignment of the grain body with its angular momentum  $\mathbf{J}$ , and to alignment of  $\mathbf{J}$  with the local magnetic field  $\mathbf{B}_0$ . If the anomalous microwave emission is rotational emission from spinning grains, it will be negligibly polarized at GHz frequencies, with  $P \lesssim 10^{-6}$  at  $\nu > 10$  GHz.

*Subject headings:* dust

## 1. Introduction

The emission from the interstellar medium (ISM) in the Milky Way and other star-forming galaxies includes strong mid-IR emission features at 3.3, 6.2, 7.7, 8.6, 11.3, 12.6, and  $17\mu\text{m}$  (see, e.g., Smith et al. 2007). The only viable explanation for this emission is a substantial interstellar population of nanoparticles with the composition of polycyclic aromatic hydrocarbons (PAHs), containing as few as  $\sim 40$  atoms (Tielens 2008). The PAHs have been identified by their characteristic IR emission features, but it is possible that nanoparticles with other compositions – such as silicates or metallic Fe – could also be abundant. For the densities and temperatures present in the ISM, nanoparticles containing fewer than  $\sim 10^3$  atoms will inevitably be spinning at  $\sim$ GHz frequencies.

The so-called anomalous microwave emission (AME) observed at 10–60 GHz was interpreted as rotational emission from rapidly-rotating nanoparticles (Draine & Lazarian 1998a,b). Given the PAH abundances and size distribution required to explain the observed mid-IR emission, it was natural to consider spinning PAHs as the source for the AME. However, a recent observational study (Hensley et al. 2016) failed to find the expected correlation of AME emission with PAH

abundance. Hensley et al. (2016) therefore suggested that spinning non-PAH (e.g., silicate or iron) nanoparticles may also be present in the ISM. Possible emission from silicate and iron nanoparticles has been further discussed by Hoang et al. (2016), Hoang & Lazarian (2016b), and Hensley & Draine (2016).

This paper examines the dynamics of dissipation in spinning interstellar nanoparticles, whether composed of hydrocarbons, silicates, or other materials. Two types of dissipation are discussed. One is the internal dissipation that allows a tumbling grain to minimize its rotational kinetic energy by aligning  $\hat{\mathbf{a}}_1$  = the principal axis of largest moment of inertia with its angular momentum  $\mathbf{J}$ . The other is the dissipation that occurs in a static magnetic field  $\mathbf{B}_0$  when  $\mathbf{J}$  is not aligned with  $\mathbf{B}_0$ . In both cases, rotational kinetic energy is converted to heat.

Dissipative processes in grains have usually been treated in the classical limit where the rotating body has many internal degrees of freedom. However, in very small grains, energy level quantization will suppress intramolecular vibration-rotation energy transfer (IVRET) and dissipation of rotational energy.

Here we examine the quantum suppression of dissipation in spinning grains. Vibration-rotation energy exchange must be suppressed when the vibrational energy level spacing  $\Delta E$  is larger than the intrinsic width  $\delta E$  of the energy levels. We estimate the suppression factor, as a function of the grain's size and vibrational energy content  $E_{\text{vib}}$ .

We calculate the implications of this quantum suppression on both the alignment of  $\mathbf{J}$  with  $\mathbf{B}_0$ , and on the alignment of the principal axis  $\hat{\mathbf{a}}_1$  with  $\mathbf{J}$ . Quantum suppression effects are extreme for the smallest nanoparticles, leading to almost total suppression of alignment of  $\mathbf{J}$  with  $\mathbf{B}_0$  for the smallest (and therefore most rapidly-rotating) grains. If the AME is rotational emission from nanoparticles, it will be essentially unpolarized.

The paper is organized as follows. Section 2 reviews the energy levels of spinning nanoparticles, and section 3 examines the distribution of vibrational modes and energy levels. Section 4 estimates the factor  $\psi_q(E_{\text{vib}})$  by which IVRET will be suppressed in a nanoparticle, as a function of the vibrational energy  $E_{\text{vib}}$  present in the nanoparticle. Section 5 concerns the quantum suppression of alignment of the grain body with  $\mathbf{J}$ . In section 6 we discuss the quantum suppression of magnetic dissipation in either paramagnetic or ferromagnetic grains. The rotation and alignment of spinning nanoparticles is calculated in section 7. In section 8 we calculate the polarization of rotational emission from spinning nanoparticles, as a function of frequency. For conditions characteristic of neutral diffuse clouds, we show that the rotational emission at frequencies  $> 1$  GHz should have very small polarization,  $\lesssim 0.01\%$ . In section 9 we calculate the degree of polarization of thermal emission from spinning nanoparticles, and the dichroic extinction contributed by such particles. The results are discussed in section 10, and summarized in section 11.

## 2. Energy Levels of a Spinning Nanoparticle

### 2.1. Rotation

Consider grains that can be approximated by spheroids, with  $I_{\parallel}, I_{\perp}, I_{\perp}$  being the eigenvalues of the moment of inertia tensor. Consider the case  $I_{\parallel} > I_{\perp}$  (i.e., oblate spheroids). Let  $J$  = the total angular momentum quantum number. In the center-of-mass frame, the total energy of the grain is

$$E_{v,J,K} = E_{v,0,0} + E_{\text{rot}} \quad (1)$$

$$E_{\text{rot}} = hc [B_v J(J+1) - (B_v - A_v) K^2] \quad , \quad (2)$$

where the “rotation constants”  $A_v$  and  $B_v$  may depend on the vibration state  $v$ , and the quantum number  $K$  is the projection of  $\mathbf{J}$  along the symmetry axis  $\hat{\mathbf{a}}_1$ . For a spheroid, the rotation constants are

$$A = \frac{\hbar}{4\pi c I_{\parallel}} \quad (3)$$

$$B = \frac{\hbar}{4\pi c I_{\perp}} \quad , \quad (4)$$

where  $I_{\parallel}, I_{\perp}$  are the moments of inertia for rotation parallel or perpendicular to the symmetry axis. An oblate spheroid ( $I_{\parallel} > I_{\perp}$ ) has  $B > A$ .

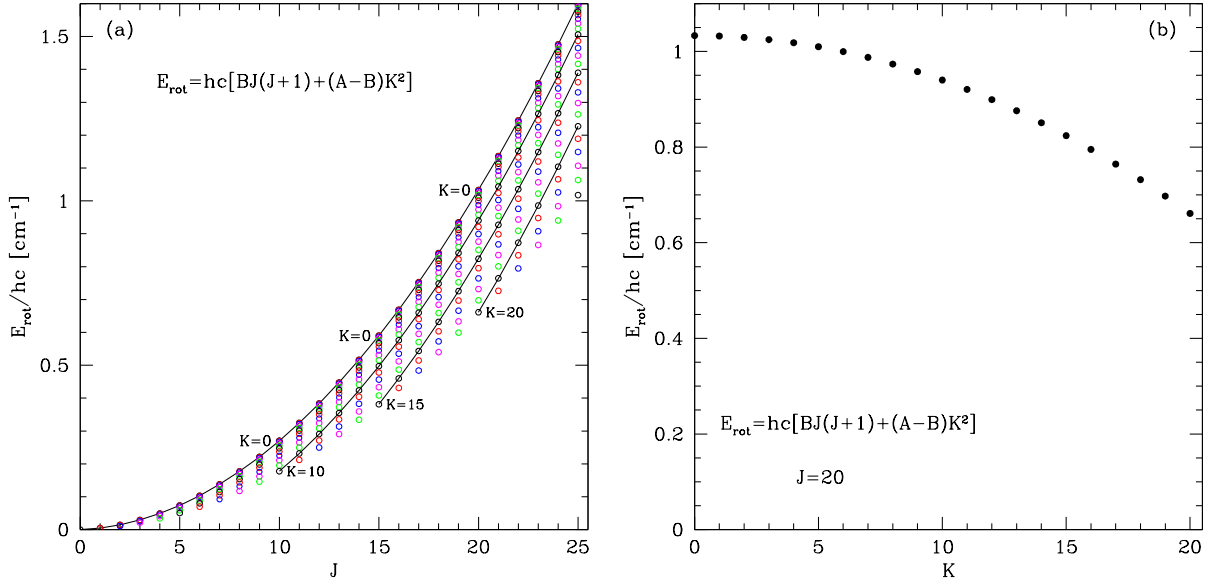


Fig. 1.— Rotational kinetic energy for an oblate spheroid with axial ratio  $b/a = 2$ , mass 800 amu, and density  $3.2 \text{ g cm}^{-3}$ . (a)  $E_{\text{rot}}$  vs.  $J$ , for different values of  $K$ . (b)  $E_{\text{rot}}$  vs.  $K$ , for  $J = 20$ .

Figure 1a shows the rotational states of an oblate spheroid with  $J \leq 25$ . For a given  $J$ , there are  $J + 1$  possible values of  $K$ , with  $K = 0$  giving the highest energy, and  $K = J$  giving the lowest energy. Figure 1b shows the energy levels for  $J = 20$ .

## 2.2. Vibration

Suppose the grain has total internal energy  $E_{v,J,K}$  in vibration and rotation. The uncertainty  $\delta E$  of the internal energy is determined by the level lifetime. If  $A_{\text{rad}}$  is the probability per unit time of a spontaneous radiative transition,  $\dot{N}_{\text{abs}}$  is the probability per unit time of absorbing a photon, and  $\dot{N}_{\text{coll}}$  is the probability per unit time of an inelastic collision with a gas particle, then

$$\delta E \approx \hbar(A_{\text{rad}} + \dot{N}_{\text{abs}} + \dot{N}_{\text{coll}}) \quad . \quad (5)$$

Radiation can be either purely rotational, or rovibrational; we write  $A_{\text{rad}} = A_{J \rightarrow J-1} + A_{\text{vib}}$ . The Einstein A coefficient for pure rotational transitions is

$$A_{J \rightarrow J-1} \approx \frac{2\omega^3}{3\hbar c^3} \mu_{\perp}^2 \quad , \quad (6)$$

where  $\omega \approx 4\pi c B_v J$ , and  $\mu_{\perp}$  is the rms electric dipole moment perpendicular to  $\mathbf{J}$  for the spinning grain. If  $\nu_{\text{rot}} = \omega/2\pi$ , then

$$A_{J \rightarrow J-1} \approx 4 \times 10^{-6} \left( \frac{\mu_{\perp}}{5 \text{ D}} \right)^2 \left( \frac{\nu_{\text{rot}}}{30 \text{ GHz}} \right)^3 \text{ s}^{-1} \quad . \quad (7)$$

Consider for the moment a spherical particle of radius  $a$ . At long wavelengths, the absorption cross section for interstellar amorphous silicate grains is (Draine & Hensley 2016)

$$C_{\text{abs}}(\lambda) \approx 9 \times 10^{-19} \text{ cm}^2 \left( \frac{100 \mu\text{m}}{\lambda} \right)^2 \left( \frac{a}{10^{-7} \text{ cm}} \right)^3 \quad ; \quad (8)$$

for this cross section, a grain with vibrational temperature  $T_{\text{vib}}$  radiates photons at a rate

$$A_{\text{vib}} = 4\pi \int C_{\text{abs}}(\nu) \frac{B_{\nu}(T)}{h\nu} d\nu \approx 2.6 \left( \frac{T_{\text{vib}}}{10^2 \text{ K}} \right)^5 \left( \frac{a}{10^{-7} \text{ cm}} \right)^3 \text{ s}^{-1} \quad (9)$$

and power

$$\dot{E}_{\text{vib}} = 4\pi \int C_{\text{abs}}(\nu) B_{\nu}(T) d\nu \approx 1.9 \times 10^{-13} \left( \frac{T_{\text{vib}}}{10^2 \text{ K}} \right)^6 \left( \frac{a}{10^{-7} \text{ cm}} \right)^3 \text{ erg s}^{-1} \quad . \quad (10)$$

In the interstellar radiation field, the nanoparticle absorbs starlight photons at a rate (see Figure 11 of Draine & Li 2001)

$$\dot{N}_{\text{abs}} \approx 5 \times 10^{-7} U \left( \frac{a}{10^{-7} \text{ cm}} \right)^3 \text{ s}^{-1} \quad , \quad (11)$$

where the dimensionless factor  $U$  is the intensity of the radiation field relative to the local interstellar radiation field (Mathis et al. 1983).

In gas of density  $n_{\text{H}}$  and temperature  $T_{\text{gas}}$ , the gas-grain collision rate is

$$\dot{N}_{\text{coll}} \approx n_{\text{H}} \left( \frac{8kT_{\text{gas}}}{\pi m_{\text{H}}} \right)^{1/2} \pi a^2 = 1.4 \times 10^{-7} \text{ s}^{-1} \left( \frac{n_{\text{H}}}{30 \text{ cm}^{-3}} \right) \left( \frac{T_{\text{gas}}}{10^2 \text{ K}} \right)^{1/2} \left( \frac{a}{10^{-7} \text{ cm}} \right)^2 . \quad (12)$$

Thus for a silicate nanoparticle with  $a \approx 5 \times 10^{-8} \text{ cm}$ , we have a level lifetime

$$\tau \approx \left[ 0.3 \left( \frac{T_{\text{vib}}}{10^2 \text{ K}} \right)^5 + 4 \times 10^{-6} \left( \frac{\nu_{\text{rot}}}{30 \text{ GHz}} \right)^3 + 6 \times 10^{-8} U + 3 \times 10^{-8} \left( \frac{n_{\text{H}}}{30 \text{ cm}^{-3}} \right) \left( \frac{T_{\text{gas}}}{10^2 \text{ K}} \right)^{1/2} \right]^{-1} \text{ s} \quad (13)$$

corresponding to a level width

$$\frac{\delta E}{hc} \approx 1.6 \times 10^{-12} \left[ \left( \frac{T_{\text{vib}}}{10^2 \text{ K}} \right)^5 + 10^{-5} \left( \frac{\nu_{\text{rot}}}{30 \text{ GHz}} \right)^3 + 2 \times 10^{-7} U + 10^{-7} \left( \frac{n_{\text{H}}}{30 \text{ cm}^{-3}} \right) \left( \frac{T_{\text{gas}}}{10^2 \text{ K}} \right)^{1/2} \right] \text{ cm}^{-1} . \quad (14)$$

The level lifetimes and widths are strongly dependent on the vibrational temperature  $T_{\text{vib}}$ . Broadening due to collisions, microwave rotational emission, and starlight absorption are of secondary importance so long as the grain has vibrational energy content corresponding to  $T_{\text{vib}} \gtrsim 20 \text{ K}$ .

### 3. Vibrational Density of States

A grain with  $N$  atoms, in its electronic ground state, has  $3N - 6$  vibrational degrees of freedom, each with vibrational quantum number  $\tilde{v}_j$ . The vibrational state of the grain is specified by the list of vibrational quantum numbers  $v = \{\tilde{v}_1, \dots, \tilde{v}_{3N-6}\}$  of the modes. Let  $N_v(E)$  be the number of distinct vibrational states  $v = \{\tilde{v}_1, \dots, \tilde{v}_{3N-6}\}$  with total vibrational energy  $E_{\text{vib}} < E$ . If the vibrational modes are approximated as a set of harmonic oscillators with frequencies  $\omega_j$ ,  $N_v(E)$  can be calculated using the Beyer-Swinehart algorithm (Beyer & Swinehart 1973; Stein & Rabinovitch 1973). We will consider silicate nanoparticles as an example, but our conclusions are insensitive to the detailed composition, and similar results would be obtained for PAHs or for Fe nanoparticles.

The spectrum of vibrational modes for silicates was discussed by Draine & Li (2001, hereafter DL01). DL01 found that the experimental specific heats (Leger et al. 1985) for basalt glass (50%  $\text{SiO}_2$ , 50% metal oxides by mass) and obsidian glass (75%  $\text{SiO}_2$ , 25% metal oxides by mass) could be reproduced if two-thirds of the modes were distributed according to a 2-dimensional Debye model with Debye temperature  $\Theta_2 = 500 \text{ K}$ , and one-third of the modes according to a 3-dimensional Debye model with Debye temperature  $\Theta_3 = 1500 \text{ K}$ . The lowest-frequency mode is estimated to have

$$\hbar\omega_1 = \frac{k\Theta_2}{2^{5/3}(N-2)^{2/3}} . \quad (15)$$

The  $(N-2)^{-2/3}$  dependence arises from the assumption that some of the modes are distributed as for a 2-dimensional Debye model.<sup>1</sup> While surprising, this model does reproduce the measured

---

<sup>1</sup> For the 3-dimensional Debye model, the lowest frequency mode would scale as  $\omega_1 \propto (N-2)^{-1/3}$ .

specific heat for bulk basalt and obsidian down to 10 K (see Fig. 2 of Draine & Li 2001). For  $\Theta_2 = 500$  K and  $N = 40$ , Eq. (15) gives  $\hbar\omega_1/hc = 10 \text{ cm}^{-1}$ . The lowest-frequency vibration will presumably be a bending or torsional mode of the nanocluster.

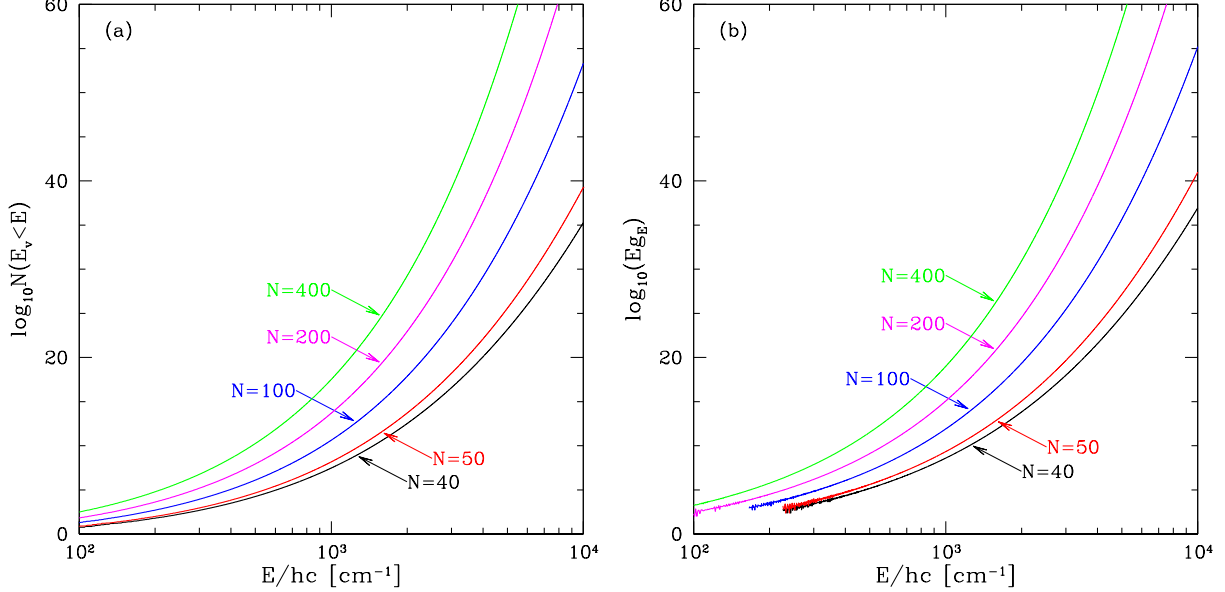


Fig. 2.— (a) The number  $N_v(E)$  of distinct vibrational states with vibrational energy  $E_{\text{vib}} < E$ , for nanosilicate clusters with  $N = 40, 50, 100, 200$  and  $400$  atoms.  $N_v(E)$  is computed using the Beyer-Swinehart algorithm and the fundamental mode spectrum estimated by Draine & Li (2001). (b)  $Eg_E$ , where  $g_E \equiv dN_v/dE$  is the vibrational density of states.

Using the mode spectrum prescription from DL01,  $N_v(E)$  is calculated using the Beyer-Swinehart algorithm. The result is shown in Figure 2a for 5 values of  $N$ . The vibrational density of states  $g_E \equiv dN_v/dE$  is shown in Figure 2b, where we have averaged over bins of width  $\Delta E/hc = 1 \text{ cm}^{-1}$ ; the “noise” at the lowest energies arises from the stepwise character of the function  $N_v(E)$ .

For vibrational energies  $E_{\text{vib}}/hc \gtrsim 5000 \text{ cm}^{-1}$ , the number of states  $N_v(E)$  is huge ( $> 10^{20}$ ), and the vibrational states can be treated as a continuum, even for a nanoparticle with as few as 40 atoms. However, for low energies, the discreteness of the vibrational spectrum can have important consequences.

#### 4. Quantum Suppression of Internal Relaxation

From Fig. 1 we see that an oblate grain with fixed  $J$  can reduce  $E_{\text{rot}}$  by increasing  $K$ , e.g.,  $K = 15 \rightarrow 16$ . However, energy conservation requires that this energy be transferred to vibrational modes. For a transition  $K \rightarrow K + 1$  to be possible, one must have  $K < J$  and there must be

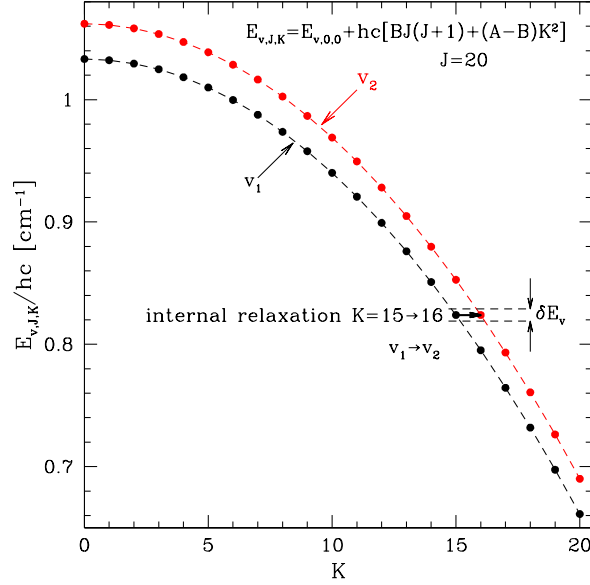


Fig. 3.— The energy difference  $E_{v,J,K} - E_{v_1,0,0}$  for  $J = 15$ . The transition  $(v_1, J, K) \rightarrow (v_2, J, K + 1)$  can take place only if  $E_{v_2,J,K+1} = E_{v_1,J,K} \pm \delta E_{\text{vib}}$ .

another vibrational state  $v_2$  such that

$$|E_{v_2,J,K+1} - E_{v_1,J,K}| \lesssim \delta E \quad , \quad (16)$$

where  $\delta E$  is the width of the energy level due to radiative or collisional broadening. Figure 3 shows such a transition. If we approximate  $B_{v_2} \approx B_{v_1}$ ,  $A_{v_2} \approx A_{v_1}$ , then Eq. (16) becomes

$$E_{v_2,0,0} = E_{v_1,0,0} + hc(B_v - A_v)(2K + 1) \pm \delta E \quad . \quad (17)$$

The probability of (17) being satisfied, i.e., for a state  $v_2$  to be available at the required energy, is approximately

$$\psi_q(E_{\text{vib}}) = 1 - \exp(-g_E \delta E) \quad , \quad (18)$$

where  $g_E$  is the vibrational density of states. For a tumbling grain, we will take the rate of vibration-rotation energy exchange (due to viscoelastic dissipation or other processes) to be the “bulk” rate multiplied by  $\psi_q(E_{\text{vib}})$ , which we will refer to as the quantum suppression factor.

Condition (17) applies to viscoelastic dissipation, which exchanges energy between kinetic energy of rotation and vibrational energy while the lattice angular momentum  $J$  remains constant. The processes of “Barnett relaxation” (Purcell 1979) – where the rotational kinetic energy can be reduced if some of the angular momentum is taken up by the system of electron spins – and “nuclear spin relaxation” (Lazarian & Draine 1999a) – where angular momentum is transferred to the system of nuclear spins – are slightly different from viscoelastic damping, because some of the

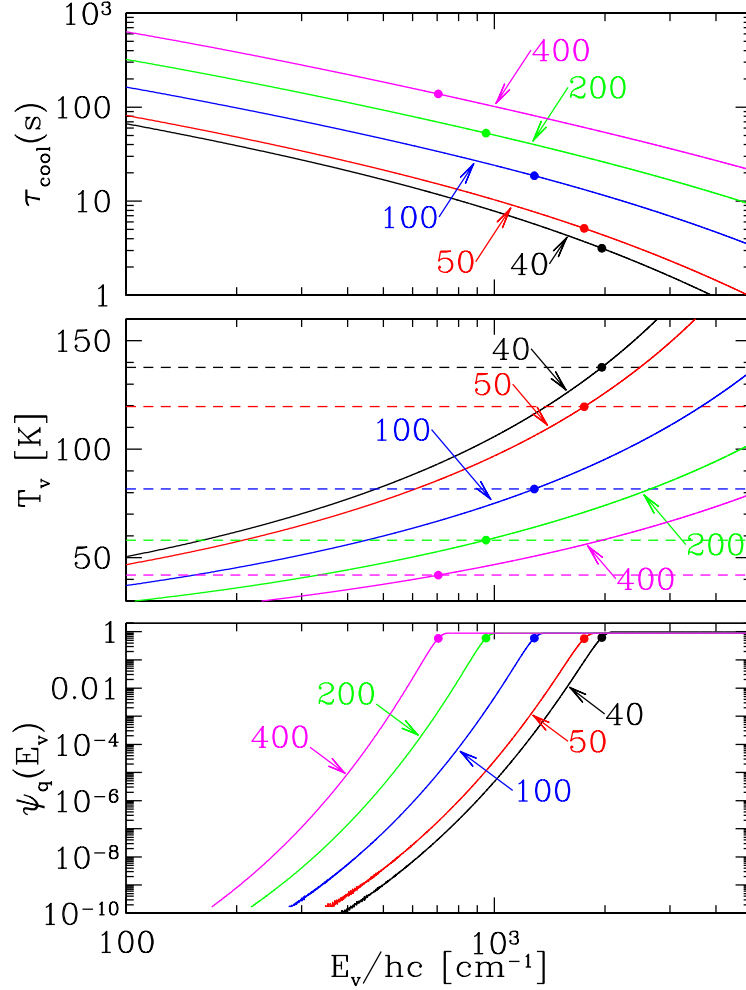


Fig. 4.— Cooling time  $\tau_{\text{cool}}$ , vibrational temperature  $T_{\text{vib}}$ , and quantum suppression factor  $\psi_q(E_{\text{vib}})$ , all as functions of the vibrational energy  $E_{\text{vib}}$ , for silicate nanoparticles containing  $N = 40, 50, 100, 200, 400$  atoms. For each case, the dot indicates the energy at which suppression of dissipation takes effect as the grain cools.

lattice angular momentum is transferred to the electron or nuclear spin systems, and the lattice angular momentum quantum number  $J \rightarrow J - 1$ . Such transitions are discussed in §6, but the same quantum suppression factor  $\psi_q$  applies.

The lower panel of Figure 4 shows the quantum suppression factor  $\psi_q(E_{\text{vib}})$  as a function of vibrational energy  $E_{\text{vib}}$  for 5 selected sizes:  $N = 40, 50, 100, 200$ , and 400 atoms. For each case, the dot shows the point where  $g_E \delta E = 1$ ; for energies below this point, IVRET will be suppressed. The middle panel shows the vibrational temperature  $T_{\text{vib}}$  as a function of  $E$ , and the upper panel shows the cooling time  $\tau_{\text{cool}} \equiv E_{\text{vib}}/|dE_{\text{vib}}/dt|_{\text{rad}}$  where  $|dE_{\text{vib}}/dt|_{\text{rad}}$  is the thermal power radiated by the grain. We define the critical temperature  $T_{\text{crit}}$  to be the vibrational temperature at which  $g_E \delta E = 1$ . Figure 5 shows the critical energy  $E_{\text{crit}}$  and critical vibrational temperature  $T_{\text{crit}}$  as a



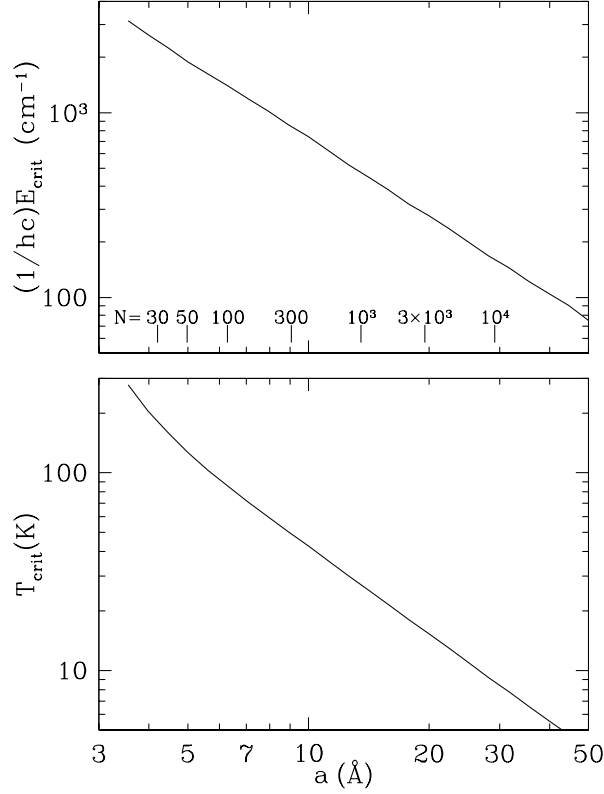


Fig. 5.— Vibrational energy  $E_{\text{crit}}$  and vibrational temperature  $T_{\text{crit}}$  where  $g_E \delta E = 1$ , above which the vibrational states can be treated as a continuum. When the grain cools below  $T_{\text{crit}}$ , internal dissipation processes are suppressed.

function of nanoparticle size.

## 5. Alignment of the Grain Body with Angular Momentum $\mathbf{J}$

Consider a grain with angular momentum quantum number  $J$ . Alignment of the grain axis  $\hat{\mathbf{a}}_1$  with  $\mathbf{J}$  is measured by

$$\langle \cos^2 \theta_{\hat{\mathbf{a}}_1 \mathbf{J}} \rangle = \frac{\langle K^2 \rangle}{J(J+1)} \quad , \quad (19)$$

where  $\theta_{\hat{\mathbf{a}}_1 \mathbf{J}}$  is the angle between  $\hat{\mathbf{a}}_1$  and  $\mathbf{J}$ . If vibration-rotation energy exchange is rapid, then the tumbling grain will have fluctuating  $K$ , with the probability of being in state  $K$  given by

$$p_K(J, T_{\text{vib}}) = C^{-1} \exp \left[ \frac{hc(B_v - A_v)K^2}{kT_{\text{vib}}(E)} \right] \quad K = -J, \dots, J \quad (20)$$

where  $C = \sum_{K=-J}^J \exp [hc(B_v - A_v)K^2/kT_{\text{vib}}]$ . The tumbling grain will have  $\langle K^2 \rangle = \sum K^2 p_K$ .

Single-photon heating of a small nanoparticle will raise it to a high temperature, resulting in

near-random orientation ( $\langle \cos^2 \theta_{\hat{\mathbf{a}}_1 \mathbf{J}} \rangle \approx 1/3$ ). So long as IVRET is rapid,  $\langle \cos^2 \theta_{\hat{\mathbf{a}}_1 \mathbf{J}} \rangle$  will gradually increase as the grain cools, and the states of lower rotational energy are increasingly favored. When the grain temperature falls to  $T_{\text{crit}}$ , the rate of internal dissipation will be suppressed. As shown in Figure 4, the onset of suppression for a nanoparticle with  $N = 100$  atoms is at  $T_{\text{vib}} \approx 75$  K, and by the time the temperature has dropped to  $\sim 65$  K the suppression factor  $\psi_q \approx 10^{-6}$ .

We have  $T_{\text{crit}} \approx 140$  K for  $N = 40$ , and  $\sim 40$  K for  $N = 400$ . Because of the rapid drop in  $\psi_q(E_{\text{vib}})$  when  $T$  drops below  $T_{\text{crit}}$ , we will approximate vibration-rotation energy exchange as rapid provided  $T > T_{\text{crit}}$ , but negligibly slow when  $T < T_{\text{crit}}$ . Thus, after absorbing a starlight photon that heats it to  $T > T_{\text{crit}}$ , the nanoparticle will have full internal relaxation, with  $p_K$  given by Eq. (20), as it cools down until reaching temperature  $T_{\text{crit}}$ , at which time the angle  $\theta_{\hat{\mathbf{a}}_1 \mathbf{J}}$  is frozen until the next starlight photon heating event, or  $\mathbf{J}$  is changed by collisions or radiation. For a grain undergoing stochastic heating by starlight photons, let  $p_E$  be the probability of being in energy bin  $E$ . Then, for grains with angular momentum quantum number  $J$

$$\langle \cos^2 \theta_{\hat{\mathbf{a}}_1 \mathbf{J}} \rangle \approx \frac{1}{J(J+1)} \left[ \sum_{E > E_{\text{crit}}} p_E \sum_K K^2 p_K(J, T_E) + \left( \sum_{E=0}^{E_{\text{crit}}} p_E \right) \sum_K K^2 p_K(J, T_{\text{crit}}) \right] . \quad (21)$$

We will evaluate  $\langle \cos^2 \theta_{\hat{\mathbf{a}}_1 \mathbf{J}} \rangle$  below after discussion of the excitation of  $J$ .

## 6. Quantum Suppression of Magnetic Dissipation and Alignment with $\mathbf{B}_0$

Now consider a nanoparticle spinning in the static interstellar magnetic field  $\mathbf{B}_0$ . The unpaired electron spins in the nanoparticle couple to  $\mathbf{B}_0$ . If  $\mathbf{J}$  has a component perpendicular to  $\mathbf{B}_0$ , then the (weak) magnetization of the grain will lag (in the grain frame, there is a rotating component of the magnetic field), and the coupling of  $\mathbf{B}_0$  to the unpaired spins will exert a torque on the spinning grain, acting to reduce the component of the total angular momentum  $\mathbf{J}$  that is perpendicular to  $\mathbf{B}_0$ . This is the Davis & Greenstein (1951) mechanism for alignment of  $\mathbf{J}$  by magnetic dissipation.

Let  $J_{\parallel \mathbf{B}}$  and  $J_{\perp \mathbf{B}}$  be the components of the angular momentum parallel and perpendicular to  $\mathbf{B}_0$ . In a large paramagnetic grain at temperature  $T_{\text{vib}}$ , magnetic dissipation will cause  $J_{\perp \mathbf{B}}$  to change at a rate

$$\left( \frac{dJ_{\perp \mathbf{B}}}{dt} \right)_{\text{DG}} = - \frac{J_{\perp \mathbf{B}}}{\tau_{\text{DG},0}} \left( \frac{T_0}{T_{\text{vib}}} \right) \quad (22)$$

$$\tau_{\text{DG},0} \equiv \frac{2\rho a^2}{5B_0^2 K_0} , \quad (23)$$

where

$$K_0 \approx 10^{-13} \left( \frac{18 \text{ K}}{T_0} \right) \text{ s} \quad (24)$$

for normal paramagnetic dissipation (Jones & Spitzer 1967). For this estimate for  $K_0$  to apply to a nanoparticle, there should be at least a few unpaired spins present in the system, so that (1) there

are spins to respond to the magnetic field, and (2) there will be spin-spin coupling as per the Jones & Spitzer (1967) estimate for  $K_0$ .

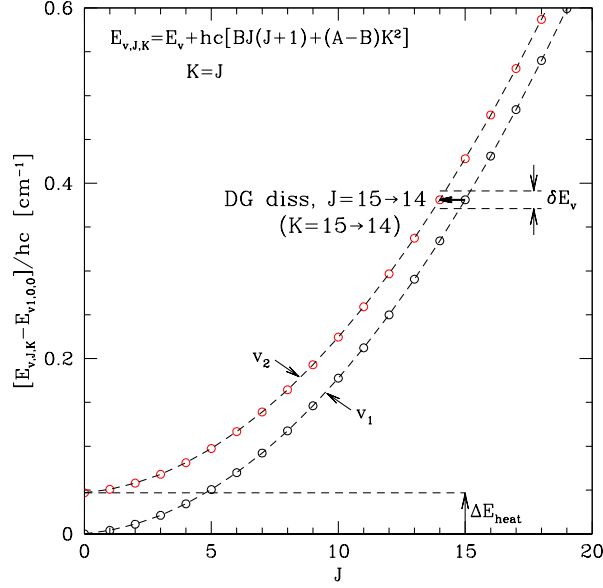


Fig. 6.— Transition from magnetic dissipation in a grain rotating in a static magnetic field.  $\Delta J = -1$ , and rotational kinetic energy is converted to heat  $\Delta E_{\text{heat}}$ . Here we show an example where the grain initially had  $J_1 = K_1 = 15$ , and  $\Delta K = -1$ . Levels with  $K = J$  are shown for vibrational states  $v_1$  and  $v_2$ .

In a single-domain ferromagnetic or ferrimagnetic grain, the spins will be spontaneously aligned, and the magnetization dynamics are quite different from the paramagnetic case. Dissipation in ferromagnetic materials at high frequencies has been discussed by Draine & Hensley (2013), with attention to Davis-Greenstein alignment. Using the Gilbert equation (Gilbert 2004) for the dynamical magnetization with Gilbert parameter  $\alpha_G \approx 0.2$ ,  $K_0$  for a pure Fe grain is estimated to be (see Draine & Hensley 2013, eq. 97)

$$K_0 \approx 3 \times 10^{-13} (1 + \cos^2 \Theta) \text{ s} \quad , \quad (25)$$

where  $\Theta$  is the angle between the spontaneous magnetization  $\mathbf{M}$  and  $\mathbf{J}$ . For paramagnetism,  $K_0 \propto 1/T_0$ , but for ferromagnetism,  $K_0$  does not depend on grain temperature (provided the temperature is well below the Curie temperature  $T_C \approx 1100 \text{ K}$ ). The estimate for  $K_0$  for metallic Fe is (coincidentally) only a factor of a few larger than the classical estimate for paramagnetism (24) at the typical grain temperature  $T_0 \approx 18 \text{ K}$ . The dependence on  $\Theta$  causes ferromagnetic dissipation to be faster if the spontaneous magnetization direction is close to  $\mathbf{J}$ , but  $(1 + \cos^2 \Theta)$  is at most a factor of two.

The time-dependent torques experienced by the unpaired spins are transferred to the lattice, which will both excite lattice vibrations (heat) and reduce the lattice angular momentum. Energy

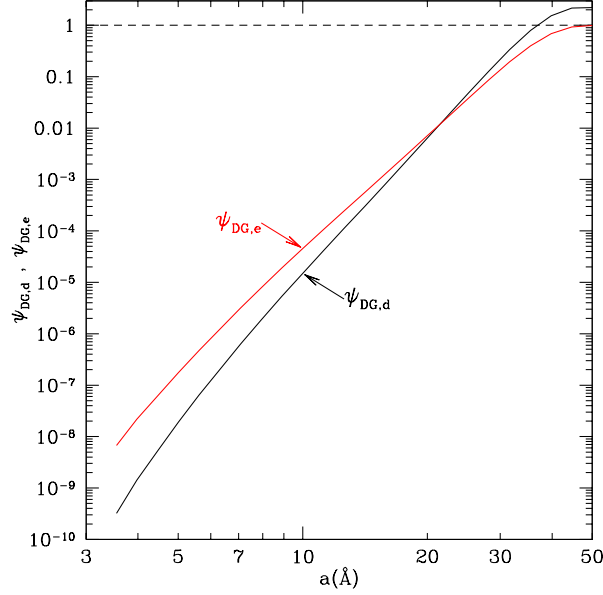


Fig. 7.— Quantum suppression factor  $\psi_{\text{DG,d}}$  for Davis-Greenstein paramagnetic alignment, as a function of radius for nanosilicate grains stochastically heated by the Mathis et al. (1983) interstellar radiation field. The related suppression factor  $\psi_{\text{DG,e}}$  for excitation of rotation perpendicular to  $\mathbf{B}_0$  is also shown.

is conserved: the decrease in rotational kinetic energy is accompanied by heating of the lattice. Figure 6 shows an example of such a transition  $J \rightarrow J - 1$ . The example shown has  $K \rightarrow K - 1$ , but other values of  $\Delta K$  can also take place.

Because energy must be conserved, magnetic dissipation can only take place if there is a suitable energy level  $v_2$  such that (see Fig. 6)

$$E_{v_2,0,0} = E_{v_1,0,0} + \Delta E_{\text{heat}} \pm \delta E \quad , \quad (26)$$

where  $\delta E$  is the “level width”, and

$$\Delta E_{\text{heat}} = 2B_v J + (A_v - B_v)(K_1^2 - K_2^2) \quad . \quad (27)$$

The likelihood of a vibrational state  $v_2$  being available so that (26) can be satisfied is again given by the function  $\psi_q(E_{\text{vib}})$  defined in Eq. (18).

For a nanoparticle heated by starlight photons,  $T_{\text{vib}}$  is a stochastic function of time, shown schematically in Figure 8. When the grain is vibrationally “hot” immediately following a photon absorption, the torques due to the static magnetic field act to *disalign*  $\mathbf{J}$  and  $\mathbf{B}_0$  (by acting to increase  $J_{\perp \mathbf{B}}^2$ ) but when  $T_{\text{vib}}$  drops below  $T_{\perp} \equiv J_{\perp \mathbf{B}}^2 / Ik$ , the dissipative torques have a net *aligning* effect (by acting to decrease  $J_{\perp \mathbf{B}}^2$ ). When the temperature falls below  $T_{\text{crit}}$ , the dissipation is strongly suppressed; the suppression factor  $\psi_q$  falls off so rapidly that the magnetic torques

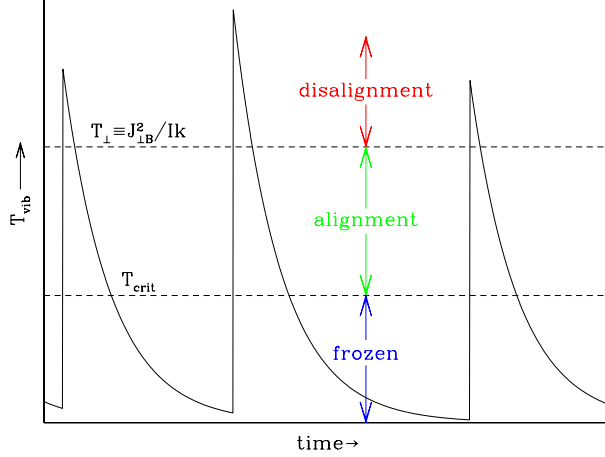


Fig. 8.— Schematic of vibrational temperature vs. time for a grain undergoing stochastic heating and radiative cooling. When the grain vibrational temperature  $T_{\text{vib}} > T_{\perp} \equiv J_{\perp}^2 / Ik \approx T_{\text{gas}}$ , the effect of the static magnetic field  $B_0$  is to increase  $J_{\perp}^2$ , acting to disalign  $\mathbf{J}$  with  $\mathbf{B}_0$ . When  $T_{\text{vib}} < T_{\perp}$ , paramagnetic dissipation tends to *reduce*  $J_{\perp}^2$ , acting to align  $\mathbf{J}$  with  $\mathbf{B}_0$ . When  $T_{\text{vib}}$  falls below  $T_{\text{crit}}$ , dissipation is suppressed, and the alignment is effectively frozen until the next heating event.

effectively cease, and we can think of the alignment as frozen until the next starlight photon is absorbed.

Averaging over the temperature fluctuations, we take the systematic aligning torque due to magnetic dissipation to be

$$\left( \frac{dJ_{\perp\mathbf{B}}}{dt} \right)_{\text{DG,d}} = -\frac{J_{\perp\mathbf{B}}}{\tau_{\text{DG},0}} \psi_{\text{DG,d}} \quad (28)$$

$$\psi_{\text{DG,d}} \equiv \sum_E p_E \left( \frac{T_{\text{vib}}(E)}{T_0} \right)^n \times \psi_q(E) \quad (29)$$

where  $n = -1$  for paramagnetism, and  $n = 0$  for ferromagnetism or ferrimagnetism.

The fluctuation-dissipation theorem implies that there must also be excitation if the lattice temperature  $T_{\text{vib}} > 0$ :

$$\left\langle \frac{dJ_{\perp\mathbf{B}}^2}{dt} \right\rangle_{\text{DG,e}} = \frac{4IkT_0}{\tau_{\text{DG},0}} \psi_{\text{DG,e}} \quad (30)$$

$$\psi_{\text{DG,e}} \equiv \sum_E p_E \left( \frac{T_{\text{vib}}}{T_0} \right)^{n+1} \psi_q(E) \quad (31)$$

where again  $n = -1$  for paramagnetism, and  $n = 0$  for ferromagnetism. It is this excitation that leads to *disalignment* of  $\mathbf{J}$  and  $\mathbf{B}_0$ . Figure 7 shows the suppression factors  $\psi_{\text{DG,d}}$  and  $\psi_{\text{DG,e}}$ . The energy distribution functions  $p_E$  for silicate nanoparticles with radii  $a$  heated by the interstellar

radiation field estimated for the solar neighborhood by Mathis et al. (1983) were calculated following Draine & Li (2001).

Papoular (2016) recently proposed that interstellar grains can be aligned with the magnetic field  $\mathbf{B}_0$  even if the grain material has zero magnetic susceptibility, because the ions and electrons in the grain will experience time-varying Lorentz forces unless the grain angular velocity  $\boldsymbol{\omega} \parallel \mathbf{B}_0$ . The mechanism proposed by Papoular also relies on dissipation of rotational kinetic energy and transfer of energy between rotation and vibration, and would be subject to the same quantum suppression factor that would apply to the paramagnetic dissipation envisaged by Davis & Greenstein (1951), or dissipation in superparamagnetic or ferromagnetic materials.

## 7. Excitation of $J$ , and Alignment of $\mathbf{J}$ with $\mathbf{B}$

We now consider the balance between excitation and damping by the various torques acting on a spinning grain. Let  $J_{\parallel\mathbf{B}}$  and  $J_{\perp\mathbf{B}}$  be the components of the grain angular momentum parallel and perpendicular to  $\mathbf{B}$ . For an individual grain,  $J_{\parallel\mathbf{B}}(t)$  and  $J_{\perp\mathbf{B}}(t)$  are stochastic variables. For an ensemble, we write

$$\frac{d}{dt} \frac{\langle J_{\parallel\mathbf{B}}^2 \rangle}{2I} \approx \frac{G}{\tau_{\text{H}}} \frac{kT_{\text{gas}}}{2} - \frac{F}{\tau_{\text{H}}} \frac{\langle J_{\parallel\mathbf{B}}^2 \rangle}{2I} - \frac{4\mu_{\perp}^2}{9c^3} \langle \omega^4 \rangle \frac{\langle J_{\parallel\mathbf{B}}^2 \rangle}{\langle J^2 \rangle} \quad (32)$$

$$\frac{d}{dt} \frac{\langle J_{\perp\mathbf{B}}^2 \rangle}{2I} \approx \frac{G}{\tau_{\text{H}}} kT_{\text{gas}} - \frac{F}{\tau_{\text{H}}} \frac{\langle J_{\perp\mathbf{B}}^2 \rangle}{2I} - \frac{4\mu_{\perp}^2}{9c^3} \langle \omega^4 \rangle \frac{\langle J_{\perp\mathbf{B}}^2 \rangle}{\langle J^2 \rangle} - \frac{(\langle J_{\perp\mathbf{B}}^2 \rangle - J_0^2) \psi_{\text{DG,d}}}{I \tau_{\text{DG},0}} \quad (33)$$

Here we approximate the grains as spherical, so that we need not consider the orientation of the body of the grain relative to  $\mathbf{J}$ . The characteristic timescale

$$\tau_{\text{H}} \equiv \frac{4\rho a}{n_{\text{H}} m_{\text{H}}} \left( \frac{\pi m_{\text{H}}}{8kT_{\text{gas}}} \right)^{1/2} \approx 2 \times 10^{11} \left( \frac{30 \text{ cm}^{-3}}{n_{\text{H}}} \right) \left( \frac{a}{10^{-7} \text{ cm}} \right) \left( \frac{100 \text{ K}}{T_{\text{gas}}} \right)^{1/2} \text{ s} \quad (34)$$

is the rotational damping time for a neutral grain in a gas of atomic H.  $F(a)$  and  $G(a)$  are dimensionless factors introduced by Draine & Lazarian (1998b), allowing for the actual rates for rotational damping and excitation arising from partial ionization of the gas, charging of the grain, and the effects of starlight and infrared emission from the grain. Note that  $\dot{N}_{\text{abs}} \tau_{\text{H}} \gg 1$  (see Eq. 11): temperature fluctuations due to stochastic heating occur on a time much shorter than the time for angular momentum variations, alignment, etc.

Loss of rotational kinetic energy from pure-rotational electric dipole radiation varies as  $\omega^4$ , but also depends on the orientation of the electric dipole moment with respect to the grain's rotation axis. Here we take  $\mu_{\perp}^2$  to be an appropriately-averaged mean square dipole moment perpendicular to the rotation axis. Following Draine & Lazarian (1998b), we suppose that

$$\mu_{\perp} \approx \beta_0 \sqrt{N} \quad , \quad (35)$$

where  $N$  is the number of atoms in the nanoparticle and  $\beta_0$  is a constant.

$F$  and  $G$  are functions of the grain charge state and radius, as well as the ionization and temperature of the gas, and have been estimated for a variety of environments (Draine & Lazarian 1998b; Ali-Haïmoud et al. 2009; Hoang et al. 2010). For the present illustration we take  $F(a)$  and  $G(a)$  calculated by Hensley & Draine (2016) for silicate particles with electric dipole moments corresponding to  $\beta_0 = 0.3$  D and cold neutral medium (CNM) conditions (see Table 1).

$\tau_{\text{DG},0}$  is the “classical” Davis-Greenstein alignment time if the grain temperature were  $T_0$ . The factors  $\psi_{\text{DG},d}$  and  $\psi_{\text{DG},e}$  include the effects of variations in temperature away from the nominal temperature  $T_0$  as well as the quantum suppression of fluctuations at temperatures below  $T_{\text{crit}}$ .  $J_0^2$  is the mean value of  $J_{\perp}^2$  if the only torques were from paramagnetic dissipation and the associated thermal fluctuations:

$$\frac{J_0^2}{2I} = \frac{\sum_E P_E \psi_q(E) \tau_{DG}^{-1} k T_E}{\sum_E P_E \psi_q(E) \tau_{DG}^{-1}} = k T_0 \frac{\psi_{\text{DG},e}}{\psi_{\text{DG},d}} \quad (36)$$

We average over  $E$  because the grain undergoes thermal fluctuations on a time short compared to the characteristic rotational damping time  $\tau_H/F$ .

We introduce dimensionless parameters

$$\beta \equiv \frac{8\mu_{\perp}^2}{9c^3} \frac{\langle \omega^4 \rangle}{\langle \omega^2 \rangle^2} \frac{k T_{\text{gas}}}{I^2} \tau_H \quad (37)$$

$$\gamma \equiv \frac{2\psi_{\text{DG},d} \tau_H}{\tau_{\text{DG},0}} \quad (38)$$

$$z_0 = \frac{J_0^2}{2IkT_{\text{gas}}} = \frac{T_0}{T_{\text{gas}}} \frac{\psi_{\text{DG},e}}{\psi_{\text{DG},d}} \quad (39)$$

and dimensionless variables

$$x \equiv \frac{\langle J_{\perp \mathbf{B}}^2 \rangle + \langle J_{\parallel \mathbf{B}}^2 \rangle}{IkT_{\text{gas}}} \quad (40)$$

$$y \equiv \frac{\langle J_{\perp \mathbf{B}}^2 \rangle}{\langle J_{\perp \mathbf{B}}^2 \rangle + \langle J_{\parallel \mathbf{B}}^2 \rangle} \quad (41)$$

Figure 9a shows  $F$ ,  $G$ ,  $\beta$ ,  $\gamma$ , and  $z_0$  as functions of grain size  $a$  for CNM conditions.

Table 1: Environmental Conditions and Grain Properties

H nucleon density	$n_{\text{H}}$	$30 \text{ cm}^{-3}$
electron density	$n_e$	$0.03 \text{ cm}^{-3}$
gas temperature	$T_{\text{gas}}$	100 K
magnetic field	$B_0$	$5 \mu\text{G}$
starlight	Mathis et al. (1983)	
silicate density	$\rho$	$3.4 \text{ g cm}^{-3}$
silicate mass/atom	21.6 amu	
electric dipole param.	$\beta_0$	0.3 D

The total rotational kinetic energy of the grain is measured by the “thermality” variable  $x$  – the ratio of the average grain rotational kinetic energy to what it would be in LTE with the gas temperature – while  $y$  measures the disalignment of  $\mathbf{J}$  from  $\mathbf{B}_0$ . In statistical steady-state, Eq. (32, 33) become

$$\tau_H \frac{d}{dt} x(1-y) = 0 = G - Fx(1-y) - \beta x^2(1-y) \quad (42)$$

$$\tau_H \frac{d}{dt} xy = 0 = 2G - Fxy - \beta x^2 y - \gamma(xy - z_0) \quad (43)$$

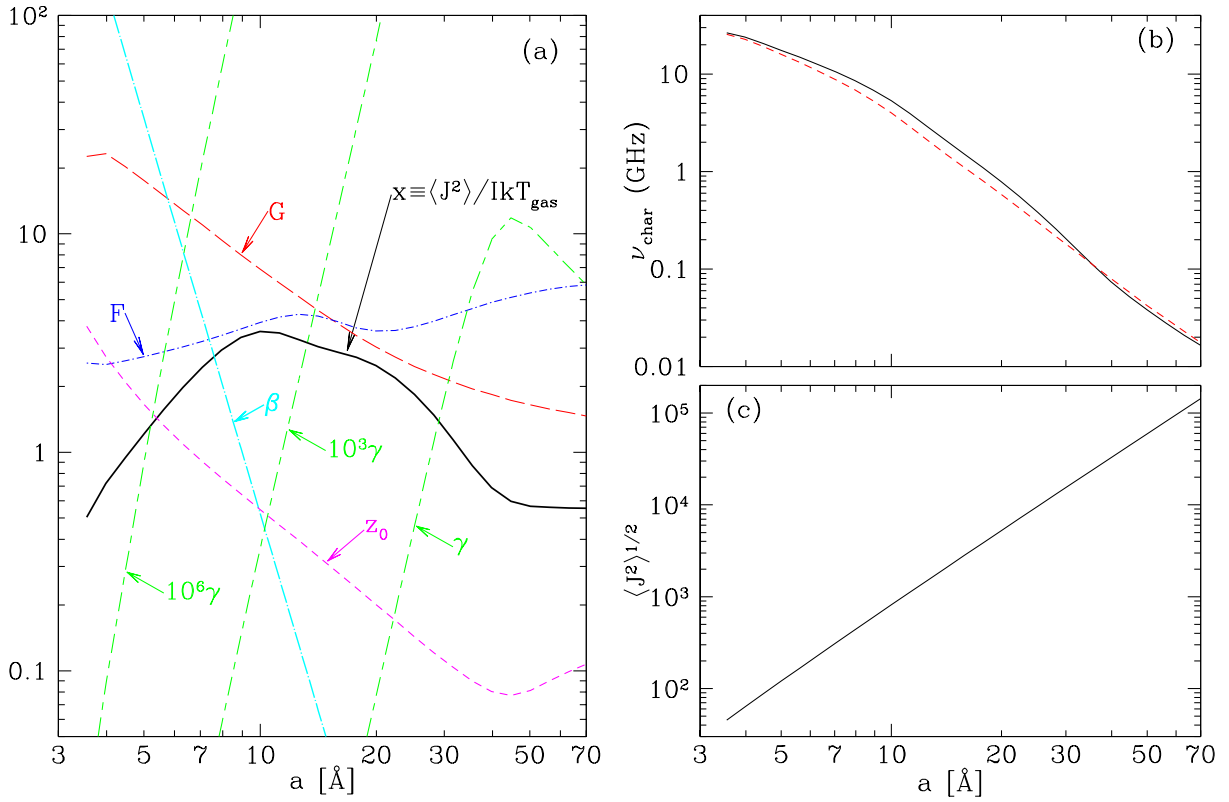


Fig. 9.— (a) The dimensionless damping and excitation factors  $F$  and  $G$ , the dimensionless parameters characterizing electric dipole damping ( $\beta$ ), magnetic dissipation ( $\gamma$ ), and magnetic excitation ( $z_0$ ), and the solution  $x$  as a function of grain size  $a$ . (b) The characteristic emission frequency as a function of grain size. Solid line: including quantum suppression of magnetic dissipation and excitation. Dashed: neglecting quantum suppression. (c) Characteristic angular momentum quantum number  $J$  vs.  $a$ .

Equations (42,43) are solved to find the steady-state values of  $x$  and  $y$  for each grain size. For an assumed  $y$  we have

$$x = \frac{[(F + \gamma y)^2 + 4\beta(3G + \gamma z_0)]^{1/2} - (F + \gamma y)}{2\beta} \quad (44)$$



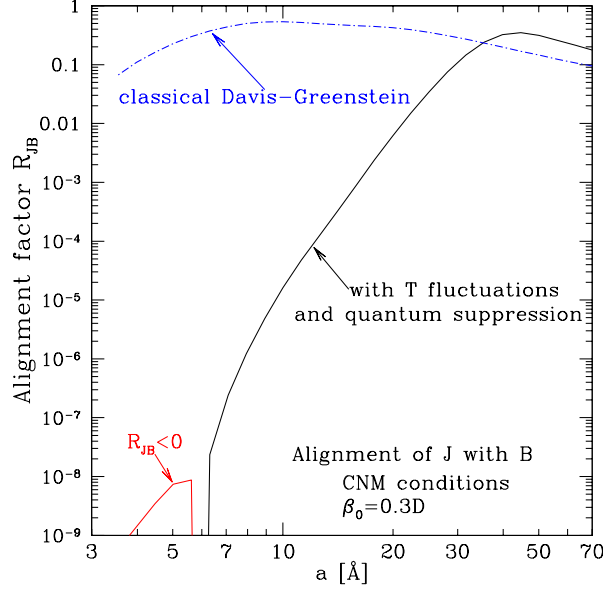


Fig. 10.— Alignment factor  $R_{\mathbf{JB}}$  for spinning grains, as a function of grain size  $a$ . Rotational emission has polarization  $P < R_{\mathbf{JB}}$ . Solid lines: Including effects of temperature fluctuations and quantum suppression of dissipation. Dot-dashed lines: “classical” treatment, neglecting  $T$  fluctuations and assuming a continuous density of states.

and for given  $x$ , we have

$$y = \frac{2}{3} - \gamma \frac{(2/3)x - z_0}{(3F + \gamma)x + 3\beta x^2} \quad . \quad (45)$$

It is straightforward to iterate to find self-consistent  $x$  and  $y$ . Figure 9a shows  $x(a)$  for CNM conditions. The rms rotation frequency for the ensemble is

$$\nu_{\text{rms}} = \frac{1}{2\pi} \left( \frac{x k T_{\text{gas}}}{I} \right)^{1/2} = \frac{1}{2\pi} \left( \frac{15}{8\pi} \frac{x k T_{\text{gas}}}{\rho a^5} \right)^{1/2} \quad (46)$$

and the characteristic emission frequency is<sup>2</sup>

$$\nu_{\text{char}} = \frac{1}{2\pi} \langle \omega^4 \rangle^{1/4} \approx \left( \frac{5}{3} \right)^{1/4} \nu_{\text{rms}} \quad . \quad (47)$$

Figure 9b shows  $\nu_{\text{char}}$  for spinning grains as a function of radius  $a$ , for CNM conditions and  $\beta_0 = 0.3D$ . We see that only the smallest grains ( $a \lesssim 8 \text{ \AA}$ ) have characteristic rotation frequencies above 10 GHz, and thus only the smallest particles contribute significantly to the AME, which typically peaks in the  $\sim 20 - 30$  GHz range (Planck Collaboration et al. 2011, 2015). Figure 9c shows the rms rotational quantum number as a function of  $a$ . Even for the smallest size, we have  $\langle J^2 \rangle \gg 1$ , justifying the classical treatment of the rotational dynamics in Eq. (32, 33).

<sup>2</sup> Because the radiated power  $\propto \omega^4$ , we take  $\omega_{\text{char}} = \langle \omega^4 \rangle^{1/4}$ . For a thermal distribution,  $\langle \omega^4 \rangle^{1/4} = (5/3)^{1/4} \langle \omega^2 \rangle^{1/2}$ .

### 7.1. Alignment of $\mathbf{J}$ with $\mathbf{B}_0$

Let  $\theta_{\mathbf{JB}}$  be the angle between  $\mathbf{J}$  and  $\mathbf{B}_0$ . The ensemble has

$$\langle \cos^2 \theta_{\mathbf{JB}} \rangle = 1 - y = \frac{1}{3} + \gamma \frac{(2/3)x - z_0}{(3F + \gamma)x + 3\beta x^2} \quad . \quad (48)$$

We define the alignment factor

$$R_{\mathbf{JB}} \equiv \frac{3}{2} \left( \langle \cos^2 \theta_{\mathbf{JB}} \rangle - \frac{1}{3} \right) = \gamma \frac{x - (3/2)z_0}{(3F + \gamma)x + 3\beta x^2} \quad , \quad (49)$$

which varies from 0 to 1 as  $\langle \cos^2 \theta_{\mathbf{JB}} \rangle$  varies from  $1/3$  (random orientations) to 1 (perfect alignment of  $\mathbf{J}$  with  $\mathbf{B}_0$ ).

For  $\gamma \ll 1$  we see that grain alignment is very small:  $R_{\mathbf{JB}} \propto \gamma \ll 1$ . Note that  $R_{\mathbf{JB}}$  can be negative when  $z_0 > (2/3)x$ . Quantum effects suppress magnetic dissipation when the grain is cold, but not during the brief intervals (following starlight heating) when it is hot. As a result, thermal fluctuations acting to *increase*  $\langle J_{\perp \mathbf{B}}^2 \rangle$  can be more important than dissipation, and cause  $R_{\mathbf{JB}}$  to go negative. However, this only occurs under conditions where quantum suppression is so effective that  $\gamma \ll 1$ , and  $|R_{\mathbf{JB}}| \ll 1$ .

Figure 10 shows  $R_{\mathbf{JB}}$  as a function of grain size, and as a function of the characteristic emission frequency  $\nu_{\text{char}}$ . The solid lines show results where the alignment is calculated including the quantum suppression of paramagnetic dissipation in small grains when  $T < T_{\text{crit}}$ .

For comparison, the alignment of  $\mathbf{J}$  with  $\mathbf{B}_0$  is also calculated assuming “classical” paramagnetic dissipation, as in the standard Davis-Greenstein treatment. These results are obtained by solving the same equations (42,43) but setting  $\psi_{\text{DG,d}} = \psi_{\text{DG,e}} = 1$  when evaluating  $\gamma$ . The classical Davis-Greenstein treatment predicts  $R_{\mathbf{JB}} \approx 3\%$  for grains spinning at  $\sim 30$  GHz, whereas when quantum suppression effects are included, the alignment factor  $R_{\mathbf{JB}}$  drops to  $\sim -10^{-9}$ .

Recent calculations of polarization from spinning silicate nanoparticles (Hoang et al. 2016) and magnetic Fe nanoparticles (Hoang & Lazarian 2016b) concluded that magnetic dissipation processes would be effective at aligning the particles, with polarization at 30 GHz predicted to be as large as  $\sim 30\%$  for silicate nanoparticles, and  $\sim 40\text{--}50\%$  for Fe nanoparticles. However, when the quantum suppression effects considered here are included, we predict minimal alignment of such particles, with extremely low polarization above  $\sim 10$  GHz.

For radii  $a \gtrsim 50 \text{ \AA}$ , the quantum suppression effects become unimportant (i.e.,  $\psi_{\text{q}} \approx 1$ ) and the present treatment coincides with classical Davis-Greenstein alignment of nanoparticles, aside from the use of fluctuating grain temperatures rather than assuming a steady temperature  $T_0 = 18 \text{ K}$ . Figure 10 shows the alignment factor  $R_{\mathbf{JB}}$  to be decreasing with increasing grain size for  $a \gtrsim 50 \text{ \AA}$  as the Davis-Greenstein alignment time  $\tau_{\text{DG},0} \propto a^2$  (see Eq. 23) becomes long compared to the rotational damping time  $\tau_{\text{H}} \propto a$  (see Eq. 34). The observed substantial alignment of the larger “classical” grains with  $a \gtrsim 0.1 \mu\text{m}$  is due to the effects of systematic torques that drive suprathermal

rotation (Purcell 1975, 1979; Lazarian & Draine 1997) including the important effects of starlight torques that can both drive  $a \gtrsim 0.1\mu\text{m}$  grains to suprathermal rotation (Draine & Weingartner 1996) as well as directly bring the grain angular momentum into alignment with  $\mathbf{B}_0$  (Draine & Weingartner 1997; Weingartner & Draine 2003; Hoang & Lazarian 2009b,a; Lazarian & Hoang 2011; Hoang & Lazarian 2016a). It is also possible that the larger grains may contain superparamagnetic inclusions that enhance alignment (Jones & Spitzer 1967; Mathis 1986; Goodman & Whittet 1995). The radiative torques that are important for  $a \gtrsim 0.1\mu\text{m}$  grains are negligible for the  $a \lesssim 0.01\mu\text{m}$  nanoparticles considered here, and other possible systematic torques due, e.g., to formation of  $\text{H}_2$  and photoelectric emission are suppressed by the “thermal flipping” phenomenon (Lazarian & Draine 1999b) and can be neglected for the nanoparticles discussed here.

## 7.2. Alignment of $\hat{\mathbf{a}}_1$ with $\mathbf{J}$

The polarization of microwave emission depends on the orientation of the grain’s angular velocity  $\boldsymbol{\omega}$ , which will not be parallel to  $\mathbf{J}$  unless  $\mathbf{J}$  is parallel to the grain’s principal axis. The alignment of  $\hat{\mathbf{a}}_1$  with  $\mathbf{J}$  is measured by

$$R_{\hat{\mathbf{a}}_1\mathbf{J}} \equiv \frac{3}{2} \left( \langle \cos^2 \theta_{\hat{\mathbf{a}}_1\mathbf{J}} \rangle - \frac{1}{3} \right) , \quad (50)$$

which again varies between 0 and 1 as the alignment of  $\hat{\mathbf{a}}_1$  with  $\mathbf{J}$  goes from random to perfect.

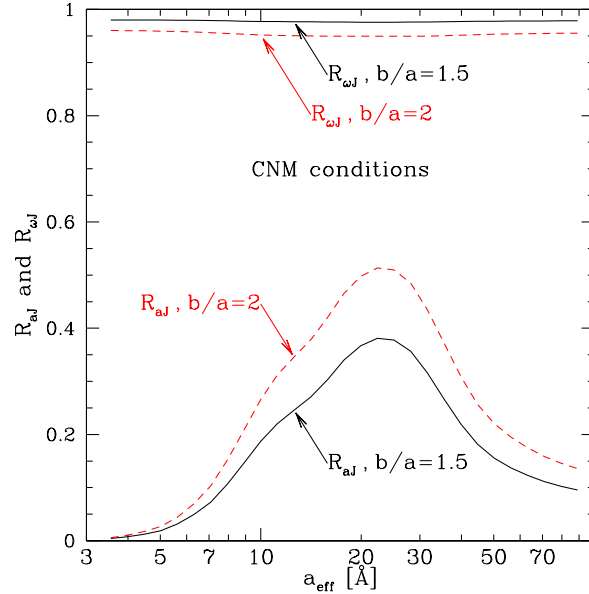


Fig. 11.— Alignment factors  $R_{\hat{\mathbf{a}}_1\mathbf{J}}$  and  $R_{\boldsymbol{\omega}\mathbf{J}}$  for oblate spheroids with  $b/a = 1.5$  and  $2$ . CNM conditions are assumed.

Recall that alignment of  $\hat{\mathbf{a}}_1$  with  $\mathbf{J}$  occurs because the spinning grain can reduce its kinetic energy by bringing the axis of largest moment of inertia into alignment with  $\mathbf{J}$ . Quantum suppression of dissipation will interfere with such alignment in very small grains. As an example, we consider oblate spheroids with axial ratio  $b/a = 2$ , i.e.,  $B_v/A_v = 2/[1 + (a/b)^2] = 1.6$ . The expectation value  $\langle \cos^2 \theta_{\hat{\mathbf{a}}_1 \mathbf{J}} \rangle$  is evaluated using Eq. (21), using the rms value of  $J$  in Figure 9c. Figure 11 shows  $R_{\hat{\mathbf{a}}_1 \mathbf{J}}(a, J)$  as a function of grain radius  $a$  for CNM excitation conditions (see Table 1). For radii  $a \lesssim 5 \text{ \AA}$ , the alignment of  $\hat{\mathbf{a}}_1$  with  $\mathbf{J}$  is minimal, although it becomes appreciable for radii  $10 \text{ \AA} \lesssim a \lesssim 50 \text{ \AA}$ .

### 7.3. Alignment of $\omega$ with $\mathbf{J}$

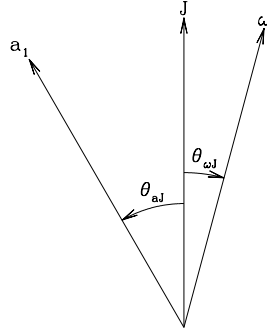


Fig. 12.— The body axis  $\hat{\mathbf{a}}_1$ , angular momentum  $\mathbf{J}$ , and angular velocity  $\omega$ .  $\hat{\mathbf{a}}_1$  and  $\omega$  both nutate around the angular momentum vector  $\mathbf{J}$ .  $\mathbf{J}$  in turn precesses around the magnetic field  $\mathbf{B}_0$  (not shown).

The electric dipole rotational emission from a single grain is 100% polarized if viewed from a direction perpendicular to the grain's instantaneous angular velocity  $\omega$ . However, if  $R_{\hat{\mathbf{a}}_1 \mathbf{J}} < 1$ , then  $\omega$  and  $\mathbf{J}$  will not be parallel, and both  $\hat{\mathbf{a}}_1$  and  $\omega$  will nutate around  $\mathbf{J}$  (see Figure 12). For an oblate spheroid, the angle  $\theta_{\omega \mathbf{J}}$  between  $\omega$  and  $\mathbf{J}$  is given by

$$\cos^2 \theta_{\omega \mathbf{J}} = \frac{[q + (1 - q) \cos^2 \theta_{\hat{\mathbf{a}}_1 \mathbf{J}}]^2}{q^2 + (1 - q^2) \cos^2 \theta_{\hat{\mathbf{a}}_1 \mathbf{J}}} \quad , \quad (51)$$

where  $q \equiv I_{\parallel}/I_{\perp} \geq 1$ . In the limit of a sphere ( $q \rightarrow 1$ ),  $\omega \parallel \mathbf{J}$ , and  $\cos^2 \theta_{\omega \mathbf{J}} = 1$  independent of the alignment of  $\hat{\mathbf{a}}_1$  with  $\mathbf{J}$ . For oblate particles with  $q > 1$ , misalignment of  $\hat{\mathbf{a}}_1$  with  $\mathbf{J}$  implies misalignment of  $\omega$  with  $\mathbf{J}$ , but this misalignment is only slight. For an ensemble of grains with angular momentum quantum number  $J$ ,

$$\langle \cos^2 \theta_{\omega \mathbf{J}} \rangle = \sum_{E > E_{\text{crit}}} p_E \sum_K \frac{[q + (1 - q) K^2 / J(J + 1)]^2}{[q^2 + (1 - q^2) K^2 / J(J + 1)]} p_K(J, T_E) + \quad (52)$$

$$\left( \sum_{E=0}^{E_{\text{crit}}} p_E \right) \sum_K \frac{[q + (1 - q) K^2 / J(J + 1)]^2}{[q^2 + (1 - q^2) K^2 / J(J + 1)]} p_K(J, T_{\text{crit}}) \quad , \quad (53)$$

where  $p_K(J, T)$  is given by Eq. (20), and we define

$$R_{\omega\mathbf{J}} \equiv \frac{3}{2} \left( \langle \cos^2 \theta_{\omega\mathbf{J}} \rangle - \frac{1}{3} \right) . \quad (54)$$

Figure 11 shows  $R_{\omega\mathbf{J}}$  as a function of grain size  $a$ , for  $b/a = 1.5$  ( $q = 1.385$ ) and  $b/a = 2$  ( $q = 1.6$ ). We see that  $R_{\omega\mathbf{J}} > 0.95$ :  $\omega$  remains quite well-aligned with  $\mathbf{J}$ , even when  $R_{\hat{\mathbf{a}}_1\mathbf{J}}$  is small.

## 8. Polarization of Rotational Emission

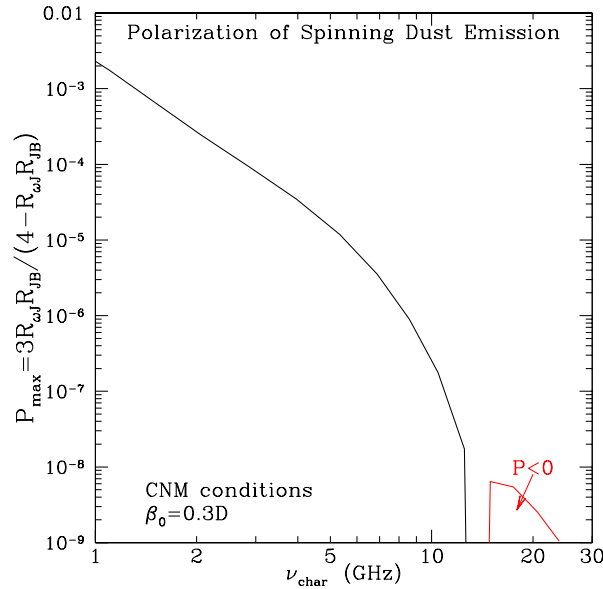


Fig. 13.— Upper limit on polarization of rotational emission as a function of characteristic frequency  $\nu_{\text{char}}$ .

If  $R_{\hat{\mathbf{a}}_1\mathbf{J}} < 1$ , a spinning grain will undergo nutation around  $\mathbf{J}$ . A spinning grain will generally have a significant magnetic moment antiparallel to  $\omega$  due to the Barnett effect (Dolginov & Mytrophanov 1976; Purcell 1979); this magnetic moment will cause  $\mathbf{J}$  to precess around  $\mathbf{B}_0$  with a period that is short enough that complete averaging over precession can be assumed. If we assume that the grain has an electric dipole moment  $\mu_{\perp}$  perpendicular to  $\omega$ , then, after averaging over rotation, nutation, and precession, one can show that the rotational emission will have fractional polarization

$$P_{\text{rot}} = \frac{3R_{\omega\mathbf{J}}R_{\mathbf{J}\mathbf{B}}}{4 - R_{\omega\mathbf{J}}R_{\mathbf{J}\mathbf{B}}} \sin^2 \Psi , \quad (55)$$

where  $\Psi$  is the angle between the viewing direction and  $\mathbf{B}_0$ . Figure 13 shows the predicted polarization as a function of frequency for viewing directions perpendicular to the static magnetic field ( $\sin^2 \Psi = 1$ ). For each frequency  $\nu$  we assume the emission to be dominated by grains with

$\nu_{\text{char}} = \nu$ . At microwave frequencies  $\nu > 5$  GHz, the predicted polarizations are extremely small. If the AME is rotational radiation from spinning dust grains, the polarization should be negligible.

## 9. Polarization of Extinction or Thermal Emission

Nonspherical grains have absorption or scattering cross sections that depend on the orientation of the grain relative to the direction and polarization of the incident radiation. In the long wavelength limit, the cross section depends on the direction of the polarization  $\mathbf{E}$  relative to the grain body, but not on the direction of propagation. We assume this to be the case in the following discussion.

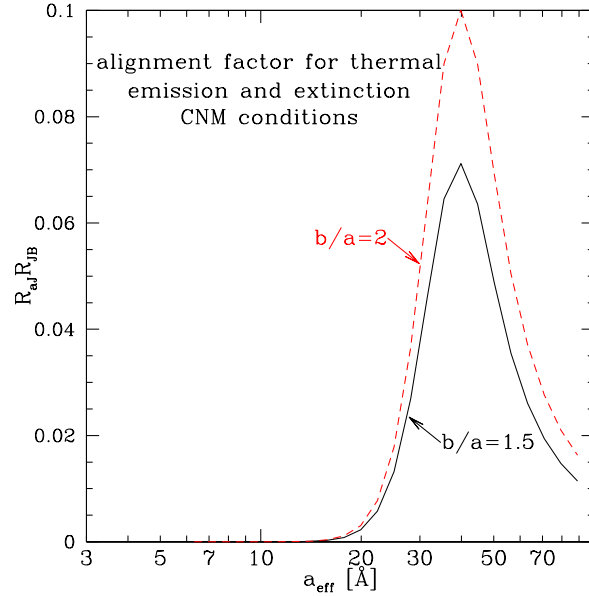


Fig. 14.— Alignment factor  $R_{\hat{\mathbf{a}}_1 \mathbf{J}} R_{\mathbf{J} \mathbf{B}}$  for dichroic extinction or thermal emission. CNM conditions are assumed.

We consider oblate spheroidal grains with symmetry axis  $\hat{\mathbf{a}}_1$ . Let  $\hat{\mathbf{e}}$  be the direction of polarization, and let  $C_{\parallel}$  and  $C_{\perp}$  be cross sections for  $\hat{\mathbf{e}} \parallel \hat{\mathbf{a}}_1$  and  $\hat{\mathbf{e}} \perp \hat{\mathbf{a}}_1$ . If we view the ensemble of grains from a direction perpendicular to  $\mathbf{B}_0$ , the ensemble of precessing and nutating grains will have mean cross sections per particle

$$\langle C \rangle_{\hat{\mathbf{e}} \parallel \mathbf{B}} = R_{\hat{\mathbf{a}}_1 \mathbf{J}} R_{\mathbf{J} \mathbf{B}} C_{\parallel} + (1 - R_{\hat{\mathbf{a}}_1 \mathbf{J}} R_{\mathbf{J} \mathbf{B}}) \frac{(C_{\parallel} + 2C_{\perp})}{3} \quad (56)$$

$$\langle C \rangle_{\hat{\mathbf{e}} \perp \mathbf{B}} = R_{\hat{\mathbf{a}}_1 \mathbf{J}} R_{\mathbf{J} \mathbf{B}} C_{\perp} + (1 - R_{\hat{\mathbf{a}}_1 \mathbf{J}} R_{\mathbf{J} \mathbf{B}}) \frac{(C_{\parallel} + 2C_{\perp})}{3} . \quad (57)$$

Thermal emission would then have polarization

$$P_{\text{th.em.}} = \frac{\langle C \rangle_{\hat{\mathbf{e}}_{\perp} \mathbf{B}} - \langle C \rangle_{\hat{\mathbf{e}}_{\parallel} \mathbf{B}}}{\langle C \rangle_{\hat{\mathbf{e}}_{\perp} \mathbf{B}} + \langle C \rangle_{\hat{\mathbf{e}}_{\parallel} \mathbf{B}}} = \frac{3R_{\hat{\mathbf{a}}_1 \mathbf{J}} R_{\mathbf{J} \mathbf{B}} (C_{\perp} - C_{\parallel})}{3R_{\hat{\mathbf{a}}_1 \mathbf{J}} R_{\mathbf{J} \mathbf{B}} (C_{\parallel} + C_{\perp}) + 2(1 - R_{\hat{\mathbf{a}}_1 \mathbf{J}} R_{\mathbf{J} \mathbf{B}})(C_{\parallel} + 2C_{\perp})} \quad . \quad (58)$$

The polarization due to dichroic extinction by a column density  $N$  of dust grains is

$$P_{\text{ext}} = \tanh(NC_{\text{pol}}) \quad (59)$$

$$C_{\text{pol}} = \frac{1}{2} (\langle C \rangle_{\hat{\mathbf{e}}_{\perp} \mathbf{B}} - \langle C \rangle_{\hat{\mathbf{e}}_{\parallel} \mathbf{B}}) = \frac{1}{2} R_{\hat{\mathbf{a}}_1 \mathbf{J}} R_{\mathbf{J} \mathbf{B}} (C_{\perp} - C_{\parallel}) \quad . \quad (60)$$

Thus for both emission and extinction the polarization is determined by the product  $R_{\hat{\mathbf{a}}_1 \mathbf{J}} R_{\mathbf{J} \mathbf{B}}$  determining the degree of grain alignment.

## 10. Discussion

Rouan et al. (1992) considered IVRET in spinning PAHs with  $N \approx 90$ , and concluded that IVRET was sufficiently rapid so that Eq. (20) should be a good approximation throughout the cooldown following absorption of a starlight photon. Quantum suppression of dissipation in grains was reconsidered by Lazarian & Draine (2000, hereafter LD00), who noted that the energy  $E_{\ell}$  of the lowest vibrationally-excited state would be appreciable in small grains, and argued that spin-lattice relaxation should be suppressed by a factor  $\propto \exp(-E_{\ell}/kT_{\text{vib}}) \ll 1$ , leading to suppression of IVRET when  $T_{\text{vib}}$  drops below  $\sim E_{\ell}/k$ . LD01 estimated that this would reduce the polarization to  $\sim 2\%$  at 20 GHz, and only  $\sim 0.5\%$  for particles small enough to spin at 30 GHz.

Sironi & Draine (2009) revisited IVRET in spinning PAHs. They argued that when the separation  $\Delta E$  of the vibrational energy levels becomes larger than  $\hbar\omega_{\text{rot}}$ , vibrational-rotational energy exchange will be suppressed. For a PAH with  $\sim 200$  C atoms, they estimated that IVRET would effectively cease when  $T_{\text{vib}}$  dropped below  $\sim 65$  K, leaving the body axis only partially aligned with  $\mathbf{J}$ .

In the present paper we have argued for a different criterion: that v-R energy transfer is suppressed when  $g_E \delta E_{\text{vib}} < 1$ , where  $\delta E_{\text{vib}}$  is the width of the energy states. Equation (18) is proposed as an estimate for the quantum suppression factor  $\psi_q$ . This criterion leads to  $\psi_q \ll 1$  for very small grains – see Fig. 7. However, Equation (18) probably *overestimates* the relaxation rate when  $g_E \delta E < 1$ : simply having a state  $v_2$  available with the appropriate energy does not ensure that the *coupling* from  $v_1$  to  $v_2$  will be fast, as there may be other “selection rules” that must be satisfied to have the energy transfer proceed at the “classical” rate. Thus, the true suppression factor  $\psi_q$  may be *smaller* than estimated from Eq. (18), and the actual degree of polarization of rotational emission may be even smaller than the already very small values estimated here, and shown in Figure 10.

The numerical values in Figures 9 and 10 were calculated for nanoparticles with the properties of amorphous silicates. However, other grain materials – in particular, PAHs or metallic Fe –

would also have quantum suppression of alignment, qualitatively similar to the silicate example shown here. Thus, if the AME is dominated by rotational emission from nanoparticles spinning at  $\sim 30$  GHz frequencies, we expect the AME to be negligibly polarized.

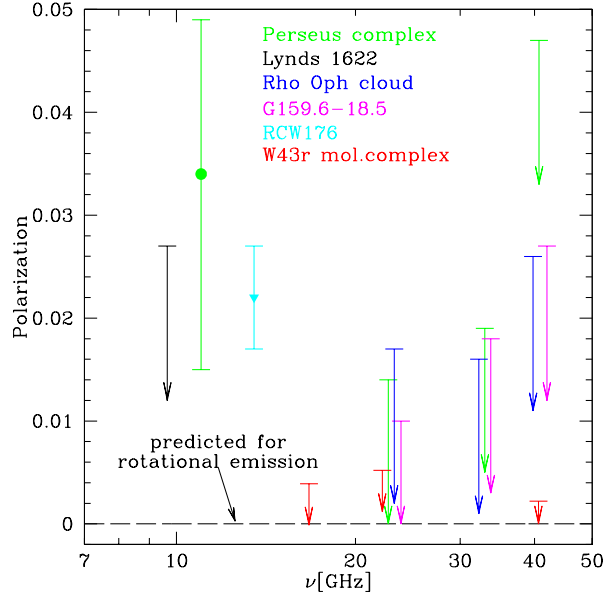


Fig. 15.— Measured polarization of AME from the Perseus molecular complex (Battistelli et al. 2006; Dickinson et al. 2011); the dark clouds Lynds 1622 (Mason et al. 2009) and  $\rho$  Oph (Dickinson et al. 2011); the HII regions G159.6-18.5 (López-Caraballo et al. 2011; Génova-Santos et al. 2015) and RCW176 (Battistelli et al. 2015); and the W43r molecular complex (Génova-Santos et al. 2016).

Our prediction of negligible polarization for rotational emission at microwave frequencies is consistent with published observations. Battistelli et al. (2006) measured the total polarization to be  $P = 3.4^{+1.5}_{-1.9}\%$  at 11 GHz for the Perseus molecular complex, but the observed polarization may be entirely due to synchrotron emission. At higher frequencies, the AME contribution from this region is consistent with zero, as are observations of the AME from the Lynds 1622 dark cloud, the  $\rho$  Oph cloud, and the HII region G159.6-18.5 – see Figure 15. A polarization  $P = 2.2 \pm 0.5\%$  was reported for the HII region RCW176 and 13.5 GHz, but this could be also be due to synchrotron emission associated with RCW176. Most recently, Génova-Santos et al. (2016) have obtained very stringent upper limits of 0.39%, 0.52% and 0.22% for the AME polarization at 16.7, 22.7, and 40.6 GHz.

At this time, our prediction of negligible polarization for rotational emission at microwave frequencies is consistent with observations.

Our modeling of the grain dynamics [Eq. (32,33)] has implicitly assumed that the damping and excitation functions  $F$  and  $G$  do not depend on the orientation of the grain angular momentum  $\mathbf{J}$  – the only dependence on orientation enters through the magnetic dissipation term in Eq.



(33). However, if the starlight illuminating the dust is anisotropic, and the grain is appreciably nonspherical, the photon absorption rate for a grain will depend on the orientation of the grain relative to the starlight anisotropy. If the grain axis  $\hat{\mathbf{a}}_1$  is aligned with  $\mathbf{J}$ , then the time-averaged photon absorption rate will in principle depend on the orientation of  $\mathbf{J}$  and on the angle  $\theta_{\hat{\mathbf{a}}_1\mathbf{J}}$ . Recognizing that  $\hat{\mathbf{a}}_1$  will be nutating around  $\mathbf{J}$ , and  $\mathbf{J}$  will be precessing around  $\mathbf{B}_0$  (the grain will generally have a magnetic moment), we do not expect  $F$  and  $G$  to have an appreciable dependence on the orientation of  $J$ , but in principle it will not be zero unless the starlight is isotropic. Because the grain angular momentum is changed by absorption of the starlight photon and the subsequent emission of infrared photons, the rotational distribution function for the dust may develop a small degree of anisotropy as the result of the starlight anisotropy. Anisotropic starlight can produce a small degree of polarization in the PAH emission features from spinning PAHs in photodissociation regions (Leger 1988; Sironi & Draine 2009). For rotational emission this effect is expected to be slight. If future observations find small but nonzero polarization for the AME, the possible contribution from this mechanism should be quantitatively evaluated.

If future observations find the AME to be polarized with  $P \gtrsim 0.01\%$  at  $\nu \gtrsim 10$  GHz, it will be evidence that the AME is not entirely rotational emission from nanoparticles, or that starlight anisotropy has generated a small degree of polarization in the rotational emission.

While quantum suppression of alignment in nanoparticles with radii  $a \lesssim 10$  Å will lead to effectively zero polarization of any rotational emission at GHz frequencies, Davis-Greenstein alignment is expected to be able to significantly align grains in the  $a \approx 30 - 50$  Å size range. The minimal degree of polarization in the far-ultraviolet (Martin et al. 1999; Whittet 2004) suggests that grains in this size range must be either nearly spherical or have low abundance.

## 11. Summary

The principal results of this paper are as follows:

1. Dissipation due to viscoelasticity or Barnett dissipation in a spinning grain is suppressed when the vibrational energy  $E_{\text{vib}}$  falls below a critical value  $E_{\text{crit}}$ : the grain's rotational kinetic energy cannot be converted to vibrational energy because there are no suitable vibrational states. This suppresses alignment of the grain body axis  $\hat{\mathbf{a}}_1$  with the grain angular momentum  $\mathbf{J}$ .
2. Paramagnetic or ferromagnetic dissipation in a nanoparticle spinning in a static magnetic field  $\mathbf{B}_0$  is also suppressed when  $E_{\text{vib}} < E_{\text{crit}}$ . This suppresses alignment of the grain angular momentum  $\mathbf{J}$  with the galactic magnetic field  $\mathbf{B}_0$ , with the greatest suppression for the smallest grains.
3. For conditions typical of the neutral ISM, the rotational emission from interstellar dust at frequencies  $\nu > 1$  GHz is expected to be negligibly polarized, with  $P < 10^{-6}$  for  $\nu > 10$  GHz.

(see Figure 13). If the anomalous microwave emission arises from spinning grains, it should be essentially unpolarized, consistent with observations to date.

4. Ordinary paramagnetic dissipation should be able to align dust grains in the  $30 - 50 \text{ \AA}$  size range. The rapid fall-off in starlight polarization in the far-ultraviolet suggests that grains in this size range are either nearly spherical or contribute only a small fraction of the far-ultraviolet extinction.

The above conclusions are not sensitive to the grain material, and apply to rotational emission from spinning PAHs, nanosilicates, or nano-Fe particles.

We thank D. Gutkowitz-Krusin for helpful discussions. This work was supported in part by NSF grant AST-1408723, and was carried out in part at the Jet Propulsion Laboratory, California Institute of Technology, under a contract with the National Aeronautics and Space Administration.

## REFERENCES

- Ali-Haïmoud, Y., Hirata, C. M., & Dickinson, C. 2009, MNRAS, 395, 1055
- Battistelli, E. S., Carretti, E., Cruciani, A., et al. 2015, ApJ, 801, 111
- Battistelli, E. S., Rebolo, R., Rubiño-Martín, J. A., et al. 2006, ApJ, 645, L141
- Beyer, T., & Swinehart, D. F. 1973, Comm. of the A.C.M., 16, 379
- Davis, L. J., & Greenstein, J. L. 1951, ApJ, 114, 206
- Dickinson, C., Peel, M., & Vidal, M. 2011, MNRAS, 418, L35
- Dolginov, A. Z., & Mytrophanov, I. G. 1976, Ap&SS, 43, 291
- Draine, B. T., & Hensley, B. 2013, ApJ, 765, 159
- Draine, B. T., & Hensley, B. 2016, in preparation
- Draine, B. T., & Lazarian, A. 1998a, ApJ, 494, L19
- Draine, B. T., & Lazarian, A. 1998b, ApJ, 508, 157
- Draine, B. T., & Li, A. 2001, ApJ, 551, 807
- Draine, B. T., & Weingartner, J. C. 1996, ApJ, 470, 551
- Draine, B. T., & Weingartner, J. C. 1997, ApJ, 480, 633
- Génova-Santos, R., Rubiño-Martín, J. A., Peláez-Santos, A., et al. 2016, ArXiv e-prints, 1605.04741

- Génova-Santos, R., Rubiño-Martín, J. A., Rebolo, R., et al. 2015, *MNRAS*, 452, 4169
- Gilbert, T. L. 2004, *IEEE Transactions on Magnetics*, 40, 3443
- Goodman, A. A., & Whittet, D. C. B. 1995, *ApJ*, 455, L181
- Hensley, B. S., & Draine, B. T. 2016, in preparation
- Hensley, B. S., Draine, B. T., & Meisner, A. M. 2016, *ApJ*, submitted [arXiv:1505.02157]
- Hoang, T., Draine, B. T., & Lazarian, A. 2010, *ApJ*, 715, 1462
- Hoang, T., & Lazarian, A. 2009a, *ApJ*, 697, 1316
- Hoang, T., & Lazarian, A. 2009b, *ApJ*, 695, 1457
- Hoang, T., & Lazarian, A. 2016a, *ArXiv e-prints*, 1605.02828
- Hoang, T., & Lazarian, A. 2016b, *ApJ*, 821, 91
- Hoang, T., Vinh, N. A., & Quynh Lan, N. 2016, *ArXiv e-prints*, 1603.05277
- Jones, R. V., & Spitzer, L. J. 1967, *ApJ*, 147, 943
- Lazarian, A., & Draine, B. T. 1997, *ApJ*, 487, 248
- Lazarian, A., & Draine, B. T. 1999a, *ApJ*, 520, L67
- Lazarian, A., & Draine, B. T. 1999b, *ApJ*, 516, L37
- Lazarian, A., & Draine, B. T. 2000, *ApJ*, 536, L15
- Lazarian, A., & Hoang, T. 2011, in *Astr. Soc. Pac. Conf. Ser. 449, Astronomical Polarimetry 2008*, ed. P. Bastien, N. Manset, D. P. Clemens, & N. St-Louis, Vol. 449, 116
- Leger, A. 1988, in *Polarized Radiation of Circumstellar Origin*, ed. G. V. Coyne, A. F. J. Moffat, S. Tapia, A. M. Magalhaes, R. E. Schulte-Ladbeck, & N. C. Wickramasinghe (Vatican Observatory), 769
- Leger, A., Jura, M., & Omont, A. 1985, *A&A*, 144, 147
- López-Caraballo, C. H., Rubiño-Martín, J. A., Rebolo, R., & Génova-Santos, R. 2011, *ApJ*, 729, 25
- Martin, P. G., Clayton, G. C., & Wolff, M. J. 1999, *ApJ*, 510, 905
- Mason, B. S., Robishaw, T., Heiles, C., Finkbeiner, D., & Dickinson, C. 2009, *ApJ*, 697, 1187
- Mathis, J. S. 1986, *ApJ*, 308, 281

- Mathis, J. S., Mezger, P. G., & Panagia, N. 1983, *A&A*, 128, 212
- Papoular, R. 2016, *MNRAS*, 457, 1626
- Planck Collaboration, Adam, R., Ade, P. A. R., et al. 2015, *ArXiv e-prints*, 1502.01588
- Planck Collaboration, Ade, P. A. R., Aghanim, N., et al. 2011, *A&A*, 536, A20
- Purcell, E. M. 1975, in *The Dusty Universe*, ed. G. B. Field & A. G. W. Cameron (New York: Neale Watson Academic), 155
- Purcell, E. M. 1979, *ApJ*, 231, 404
- Rouan, D., Leger, A., Omont, A., & Giard, M. 1992, *A&A*, 253, 498
- Sironi, L., & Draine, B. T. 2009, *ApJ*, 698, 1292
- Smith, J. D. T., Draine, B. T., Dale, D. A., et al. 2007, *ApJ*, 656, 770
- Stein, S. E., & Rabinovitch, B. S. 1973, *J. Chem. Phys.*, 58, 2438
- Tielens, A. G. G. M. 2008, *ARA&A*, 46, 289
- Weingartner, J. C., & Draine, B. T. 2003, *ApJ*, 589, 289
- Whittet, D. C. B. 2004, in *Astr. Soc. Pac. Conf. Ser. 309, Astrophysics of Dust*, ed. A. N. Witt, G. C. Clayton, & B. T. Draine (San Francisco, CA: ASP), 65